Available online at www.sciencedirect.com
ScienceDirect
International Journal of Multiphase Flow 32 (2006) 1386–1396
International Journal of Multiphase Flow
www.elsevier.com/locate/ijmulflow

Brief communication

Turbulence attenuation by small particles in the absence of gravity

W. Hwang *, J.K. Eaton

Department of Mechanical Engineering, Stanford University, Stanford, CA 94305, USA

Received 16 May 2005; received in revised form 20 June 2006

Keywords: Turbulence attenuation; Homogeneous isotropic turbulence; Micro-gravity

1. Introduction

Some examples of particle-laden turbulent flows that can be found in nature and industry include dust storms, chemical reactors, and pollutant abatement systems. In these type of flows particles are not only dispersed by the turbulence but they may also affect it in such a way that the carrier-phase turbulence level may be modified. Depending on the flow conditions and particle characteristics, augmentation and attenuation of turbulence levels have both been observed. Turbulence attenuation can become a problem if high turbulence levels are required, in areas such as heat transfer and mixing. Kulick et al. (1994) and Paris and Eaton (2001) have shown that the carrier-phase turbulence level can be attenuated up to 80% by a dilute dispersion of particles that has negligible volume fraction. The addition of an extra phase to a turbulent flow poses a very complex problem, however, and it is still not clear what causes this phenomenon of turbulence attenuation.

Previous researchers have attempted to use optical measurements in simple flows to study this problem. Parthasarathy and Faeth (1990), Mizukami et al. (1992) and Chen et al. (2000) created stationary homogeneous turbulence by dropping particles through stagnant water, air, and a counterflowing upward wind tunnel, respectively. The carrier-phase velocity fluctuations depended only on the viscous dissipation rate, which was obtained from the potential energy loss of particles and particle drag. Grid-generated turbulence has also been investigated. Schreck and Kleis (1993), Geiss et al. (2004) and Poelma et al. (2006) observed turbulence modification using laser Doppler velocimetry (LDV), phase Doppler anemometry (PDA), and particle image velocimetry/particle tracking velocimetry (PIV/PTV), respectively. Nishino et al. (2004) created a nearly stationary dispersion of particles using an upward water flow and eliminated the transfer of potential to kinetic energy of settling particles.

The ideal environment to study turbulence attenuation by particles would be in stationary homogeneous and isotropic turbulence without mean flow, in the absence of gravity so a stationary dispersion of particles

* Corresponding author. Present address: Engine Combustion Department, Combustion Research Facility, Sandia National Laboratories, P.O. Box 969, MS9053, Livermore, CA 94551, USA. Tel.: +1 925 294 6092; fax: +1 925 294 1004.
E-mail address: wthwang@stanfordalumni.org (W. Hwang).

0301-9322/$ - see front matter
doi:10.1016/j.ijmultiphaseflow.2006.06.008

can be created. Since this is very difficult to realize in a laboratory setting, several researchers have relied on numerical simulations. Squires and Eaton (1990) and Boivin et al. (1998) used direct numerical simulations (DNS) and Boivin et al. (2000) used large eddy simulations (LES) to examine such flows, and found that the turbulence kinetic energy and dissipation rate decreased with increasing particle loadings, while the energy spectra increased at high wavenumbers relative to low wavenumbers. Fallon and Rogers (2002) were recently able to experimentally create such a flow on NASA's KC-135 parabolic aircraft using fans mounted in a chamber. However, their focus was on particulate-phase measurements of particle dispersion and not carrier-phase measurements of turbulence attenuation.

The goal of this study was to experimentally investigate the ideal case of attenuation of stationary homogeneous and isotropic air turbulence without mean flow (fluid velocity $u = u'$) by a uniformly dispersed stationary array of heavy particles (particle velocity $v = v'$). More specifically, the following conditions were considered. The particulate phase was small spherical monodisperse glass beads, where the ratio between particle diameter and fluid Kolmogorov length scale $d_p/\eta \sim 1$, particle-to-fluid density ratio $\rho_p/\rho_f \sim 2000$, particle Stokes number (based on the fluid Kolmogorov time scale) $St_k \sim 140$, and particle Reynolds number $Re_p \sim 10$. The flow was dilute and had a negligible particle volume fraction $\alpha_p \sim 10^{-4}$, but non-negligible particle-to-fluid mass loading ratio $\phi \sim 0.1$, which corresponded to total number of particles $N_p \sim 10^6$ and inter-particle spacing $l_p \sim 20d_p$.

A parallel experiment was performed in ordinary terrestrial gravity. That work has already been reported in Hwang and Eaton (2006). The purpose of this brief communication is to specifically describe the different experimental procedures and data analysis techniques required for the microgravity experiments, and to present and discuss the differences in the experimental results. Only a short description of the main apparatus is given, and the reader is referred to Hwang and Eaton (2004a, 2006) for more details.

2. Experimental setup

The turbulence was created in a sealed chamber, which has been described in detail by Hwang and Eaton (2004a). The experiments were conducted in a free-floating environment aboard NASA's KC-135 parabolic flight aircraft to eliminate the effects of gravity. The turbulence chamber and particle image velocimetry (PIV) system were housed in a sturdy free-floating rack, while the computer and other electronics had to be housed in a stationary rack. Details of the experimental setup can be found in Hwang and Eaton (2004b).

2.1. Experimental facility and procedures

The KC-135 experiences fluctuations in g-levels, up to 0.1 g (Groszmann, 2001), due to vibrations of the body of the plane as it free falls. This "g-jitter" can mask the particle motion produced by the fluid turbulence in our experiments, so the main apparatus was free-floated. Although the duration of micro-gravity in each parabola was reduced, as the rig tended to float into the walls and ceiling of the cabin, the g-levels were greatly reduced to the order of milli-g and smaller.

The free-floating apparatus, depicted in Fig. 1(a), housed the turbulence chamber, camera, laser, optics rail, flow seeder, and accelerometer. The turbulence chamber is a sealed symmetric Plexiglas box with each side being 410 mm and the corners cut off to make it nearly internally spherical. Homogeneous and isotropic turbulence with small mean flow was created by eight synthetic jet actuators mounted on the corners, which used loudspeakers that had random frequency (centered at 100 Hz) and phase sine waves sent to them. The PIV system consisted of a Continuum Minilite PIV dual-head Nd:YAG laser (25 mJ/pulse at 532 nm), sheet-creating optics mounted on an optical rail, Kodak ES1.0 10 bit CCD (1018×1008 resolution) camera, and fluidized bed seeder. A Crossbow CXL01LF3 accelerometer that had a range of ± 1 g measured the vertical acceleration. The accelerometer measurements determined the validity of the data, as spikes would appear when the rack bumped into a wall or ceiling, or when the NASA flight crew touched it. The rack was made from aluminum 80/20 components and covered with aluminum panels to prevent laser light from escaping. It is shown free-floating in Fig. 1(b).

A second rack was bolted securely to the cabin floor and housed the laser power supplies, Phast PLB-Amp8 power amplifier, computer, monitor, keyboard, computer interface box, and the random frequency sine wave

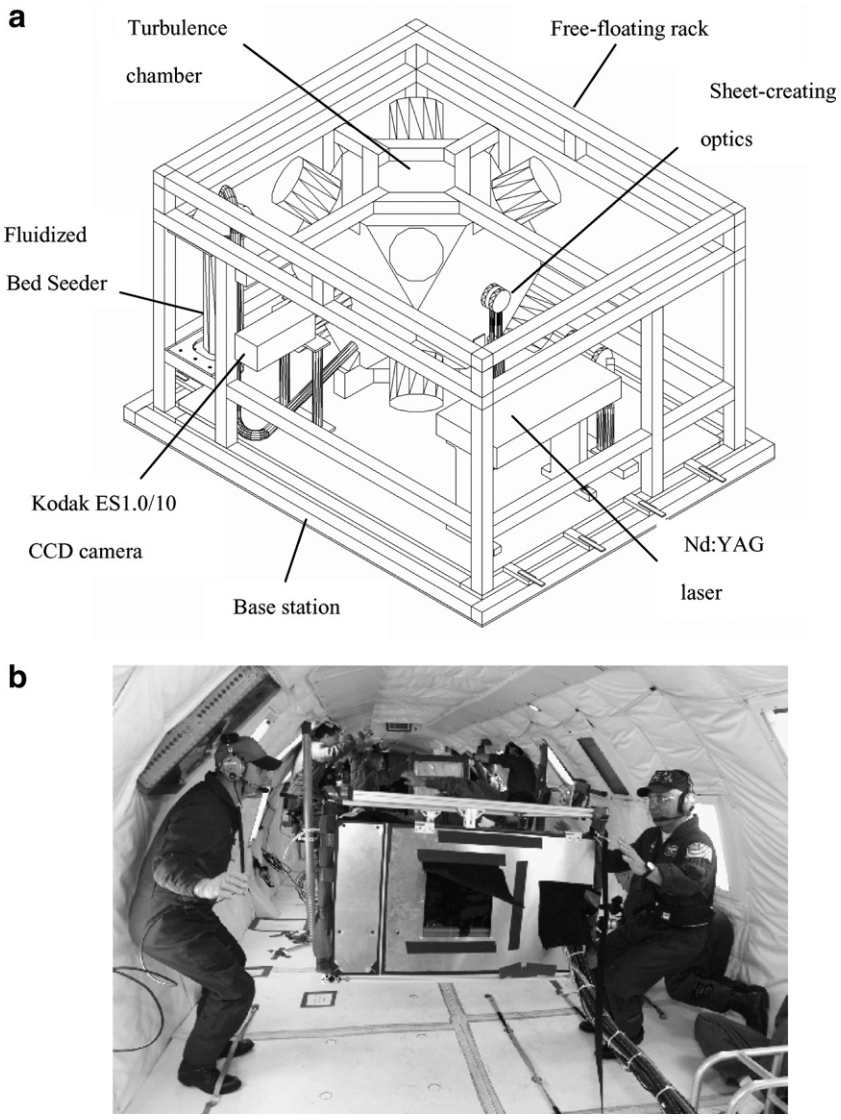

Fig. 1. (a) Free-floating rack clamped onto the base station. *Counter-clockwise from front*: Continuum Minilite Nd:YAG laser, sheet-creating optics, turbulence chamber, fluidized bed seeder, and Kodak ES1.0/10 CCD camera. (b) Free-floating rack floating in micro-gravity within NASA's KC-135.

generator. A breathing air K-bottle, which was used to supply compressed air to the fluidized bed seeder, was also fixed to the cabin floor. The electrical wires, laser cooling water hoses, and air hoses were tied together and connected to the free-floating rig as an umbilical.

Two-dimensional digital PIV was used to obtain velocity measurements at the center of the chamber for a $40 \times 40 \times 0.5\ \text{mm}^3$ region. Air seeded with 0.3 μm alumina tracer particles flowed into the chamber from the fluidized bed seeder and exited the chamber through a high efficiency inert air filter, which prevented the seed from escaping. The seeder was turned off well before commencing measurements. Images were acquired by an EPIX PIXCI-D frame grabber board and temporarily stored in 220 MB of computer memory before being saved onto the hard drive during the 2 g climbing portion of the parabolas. The 450 MHz Pentium II desktop computer synchronized the laser, camera, and synthetic jet actuators through LabVIEW.

The glass particles were eliminated from the images using a spatial median filtering technique (Kiger and Pan, 2002) to obtain PIV measurements of the gas phase from the flow tracers. Hwang and Eaton (2004b) demonstrated that the effects of particle cross-talk were small with this technique. The PIV code was written

in Matlab by Han (2001) and incorporated recursive interrogation window offset and window reduction to increase the spatial resolution, accuracy, and data yield rate. The final window size was limited to 64×64 pixels with 50% overlap (resulting in a map of 29×29 velocity vectors). Higher spatial resolution was not possible due to relatively low seeding density. Remnant spurious vectors at the final iteration were not used when calculating the statistics. A Gaussian estimator was used to obtain sub-pixel accuracy for the displacements, which had uncertainty of approximately ± 0.2 pixels.

A new set of glass particles corresponding to a certain mass loading was put into the turbulence chamber before each flight. While the plane climbed at 2 g for about 1 min, the fluidized bed seeder was turned on briefly to provide flow tracers and then the synthetic jet actuators were turned on. As the KC-135 dived into micro-gravity (which lasted about 25 s), the free-floating rack was lifted, and to get the particles off of the floor of the chamber, the rack was initially tapped on the bottom and also shaken. After the particles were dispersed, the rack was stabilized and released, and PIV images were taken at 4 Hz. The rack was pulled down to the cabin floor before the plane exited the micro-gravity portion of the parabola, giving typically 10–20 s of data collection for each parabola.

2.2. Particle characteristics and mass loading

The glass particles were obtained from Mo-Sci Specialty Products. The mean diameter, d_p, was measured to be 160 μm with a standard deviation of 15.1 μm using a Coulter counter. The density of the particles, ρ_p, was given as 2500 kg/m^3. The particle time constant is

$$\tau_p = \frac{\rho_p d_p^2}{18\mu} \frac{1}{1 + 0.15 Re_p^{0.687}} \tag{2.1}$$

where μ is the kinematic viscosity of air and Re_p is the particle Reynolds number. The particle Reynolds number was defined using the fluctuating fluid velocity (since the particles are relatively stationary) and had a value of approximately 10. The particle time constant was calculated to be 110 ms, which gives a Stokes number based on the Kolomogorov time scale of the unladen flow, $St_k = \tau_p/\tau_k$, of 140.

The particle mass loading, ϕ, was defined as the ratio of the mass of suspended particles to the mass of air in the turbulence chamber. A measured quantity of glass particles was put into the chamber before each flight. For example, an intended mass loading of 30% corresponded to 19 g and about 0.25 fl oz. of particles. However, not all of the particles became suspended, because some of the particles stuck to the floor of the chamber due to electrostatic effects and a small amount of particles got into the synthetic jet actuator plenums. The mass loading was therefore obtained from the calibration method developed by Hwang and Eaton (2004b) which used the experimental facility in the lab, without the synthetic jet actuators operating.

First, the particles were dropped down through a long chute from a screw feeder into the chamber. The particle mass flux, $\dot{m}_p$, was obtained at five different screw feeder settings by measuring the accumulating mass of particles at the bottom of the chamber using a load cell. The mass increased very linearly with time, and the slope of each line corresponded to the particle mass flux. A control volume was taken around an imaginary cylinder in the chamber having a diameter equal to that of the particle chute, and height, H, equal to that of the chamber. The mass loading ratio of this cylindrical control volume could then be calculated as $\phi = M_p/M_a$, where M_p is the mass of dispersed particles and M_a is the mass of air in the control volume. The mass of dispersed particles was calculated as $M_p = \dot{m}_p H/v_t$, where v_t is the particle terminal velocity, which was measured to be 1.2 m/s in the chamber using particle tracking velocimetry (PTV) implemented using the same optical setup used for PIV. The measured particle velocity was slightly larger than the terminal velocity calculated from the particle time constant, $v_t = \tau_p g = 1.1$ m/s. The final step involved taking images of the settling particles and obtaining the average number of particles per image, n_p, for each screw feeder setting and corresponding ϕ. The mass loading ratio, ϕ, could thus be written as

$$\phi = 6.55 \times 10^{-4} n_p + 3.97 \times 10^{-3} \tag{2.2}$$

For the actual micro-gravity experiments where the synthetic jet actuators were running, ϕ was obtained from (2.2) by counting the number of particles per image. The uncertainty in the mass loading, $\delta\phi$, was calculated

from the uncertainty in the average number of particles, δn_p, using (2.2). For a small number of images, the uncertainty in the average number of particles per image, n_p, is large, and the uncertainty in ϕ is therefore inherently large.

3. Results and discussion

The number of valid experimental data sets was limited by practical difficulties. Due to equipment failure in micro-gravity, only one out of the five flights resulted in a good series of data sets. Each flight consisted of approximately 40 parabolas, but the experiments could only be conducted every other parabola, as it took a finite amount of time to transfer the PIV images from computer memory to hard drive. The NASA technicians occasionally nudged the free-floating rack to keep it near the center of the work space and also grabbed it if its trajectory appeared dangerous. These events were easily detected in the accelerometer data. PIV data from a given parabola were only deemed valid as long as the accelerometer continuously had vertical acceleration levels of 0.01 g or less.

A small amount of particles became lodged in the synthetic jet actuator plenums or got stuck in the corners of the test chamber after each parabola. Therefore, the mass loading varied over the course of the flight. Each parabola was treated as a separate experiment. The particle mass loading and the turbulence properties were evaluated using all the valid image pairs for a given parabola. Six of the parabolas had a sufficient number of valid image pairs to provide useful statistics. These six included 18, 25, 7, 8, 19, and 10 valid image pairs. The uncertainty in the particle mass loading estimate depended on the number of image pairs available, but was typically less than ± 0.02. More detailed results are presented for the first parabola, which was chosen because both the measured mass loading and the number of valid image pairs were relatively large.

There was some concern that particles accumulating in the synthetic jet actuator plenums may have interfered with the experiments. However, only a very small amount of particles ($\ll 1$ g) became lodged in each plenum, and this had a negligible effect on the energy input into the turbulence. During the terrestrial experiments (Hwang and Eaton, 2006), particles flowed continuously into the apparatus and accumulated on the floor of the chamber. The amount of particles accumulated in the lower plenums by the end of a typical experiment was very much greater than during the microgravity experiments. Nonetheless, this much larger accumulation caused at most a 5% reduction in the single-phase turbulent kinetic energy in the chamber (Hwang and Eaton, 2006).

3.1. Turbulence attenuation

The micro-gravity results were compared with and normalized by base unladen flow measurements of approximately 200 image pairs taken in the lab (on the ground) at the same experimental conditions before the micro-gravity flights. The unladen flow turbulent root-mean-square (rms) velocities in the horizontal and vertical directions were fairly large and nearly identical at $u_{1,\mathrm{rms}} = 0.928$ m/s and $u_{2,\mathrm{rms}} = 0.936$ m/s. This was an indication that the turbulence was energetic and isotropic. The corresponding value of q^2, twice the turbulence kinetic energy, was estimated to be 2.62 $\mathrm{m}^2/\mathrm{s}^2$ from

$$q^2 \equiv u_{i,\mathrm{rms}} u_{i,\mathrm{rms}} \cong 3\frac{u_{1,\mathrm{rms}}^2 + u_{2,\mathrm{rms}}^2}{2} \tag{3.1}$$

assuming isotropy and spatially averaging $q^2(x_1, x_2)$. Local turbulence statistics can be spatially averaged if the turbulence is homogeneous. Fig. 2 shows that the distribution of $q^2(x_1, x_2)$ normalized by its spatial average $\langle q^2 \rangle = 2.62$ $\mathrm{m}^2/\mathrm{s}^2$ had values within 0.8–1.2 for 200 image pairs, indicating that the turbulence was homogeneous. Hwang and Eaton (2004a) showed that $q^2(x_1, x_2)/\langle q^2 \rangle$ only varied within 0.9–1.1 for 1000 image pairs. The energy production due to mean velocity gradients was estimated to be at most 5.3 $\mathrm{m}^2/\mathrm{s}^3$. This was much smaller than the viscous dissipation rate, ε, estimated to be 24.6 $\mathrm{m}^2/\mathrm{s}^3$ using a method proposed by Sheng et al. (2000), which is based on an LES analogy. This was additional evidence that the turbulence was homogeneous. The Taylor microscale and associated Reynolds number of the unladen flow are given as

$$\lambda \cong \left(\frac{5\nu q^2}{\varepsilon}\right)^{1/2}, \quad Re_\lambda \cong \frac{\lambda (q^2/3)^{1/2}}{\nu} \tag{3.2}$$

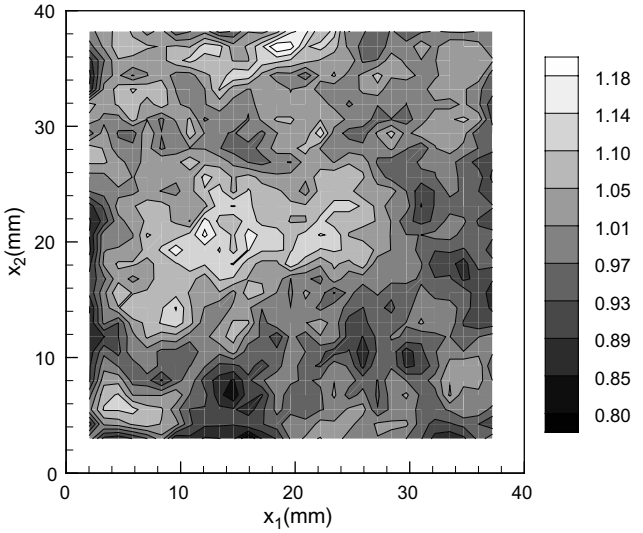

Fig. 2. Spatial map of $q^2(x_1, x_2)/\langle q^2 \rangle$ in unladen turbulence.

and had values of 2.8 mm and 176, respectively. The Kolmogorov length and time scale are defined as

$$\eta \equiv \left(\frac{\nu^3}{\varepsilon}\right)^{1/4}, \quad \tau_k \equiv \left(\frac{\nu}{\varepsilon}\right)^{1/2} \tag{3.3}$$

and had values of 0.11 mm and 0.78 ms, respectively.

Because of the finite spatial resolution of the PIV system, the turbulence kinetic energy may have been underestimated due to filtering of small-scale motions. This effect was estimated using the model energy-spectrum function given by Pope (2000)

$$E(k) = C\varepsilon^{2/3}k^{-5/3}\left(\frac{kL}{[(kL)^2 + c_L]^{1/2}}\right)^{5/3+p_0} \exp\{-\beta\{[(k\eta)^4 + c_\eta^4]^{1/4} - c_\eta\}\} \tag{3.4}$$

where k is wavenumber and L is a large eddy length scale. The coefficients are given as $C = 1.5$, $\beta = 5.2$, $p_0 = 2$, $c_L = 6.78$ and $c_\eta = 0.40$ for high Re_λ. This spectrum is similar for various Re_λ when scaled with the longitudinal integral length scale L_{11}, which was estimated to be about 10 mm from two-point longitudinal velocity correlation functions (Hwang and Eaton, 2004a). Integration of the spectrum up to the largest normalized wavenumber (corresponding to the smallest resolvable length scale) $kL_{11} = 26$ shows that the measurements captured approximately 90% of the turbulent kinetic energy. Slight differences with Re_λ and uncertainty in the estimate of L_{11} make this value only a rough approximation. However, this analysis does indicate that the measurements captured most of the energy in the flow.

The turbulence kinetic energy was spatially averaged over all measurement locations within the image and also averaged over all the image pairs of a given parabola. The uncertainty in this measurement was dominated by the statistical uncertainty due to the relatively small number of image pairs. The uncertainty in each turbulence kinetic energy measurement was estimated by dividing the baseline unladen data set (for which 200 image pairs were available) into groups of images that had the same number of images as the particular micro-gravity data set of interest. The variation in turbulence kinetic energy among the groups was taken as the uncertainty for the turbulence kinetic energy for each micro-gravity data set.

The turbulence kinetic energy results are presented in Fig. 3 normalized by the base unladen turbulence kinetic energy. Also shown are data from ground-based experiments in the same apparatus where particles fell through the flow (Hwang and Eaton, 2006), measurements from the centerplane of a vertical fully developed channel flow apparatus (Paris and Eaton, 2001), and results of two numerical simulations of isotropic particle-laden turbulence (Squires and Eaton, 1990; Boivin et al., 1998). All these results show the same

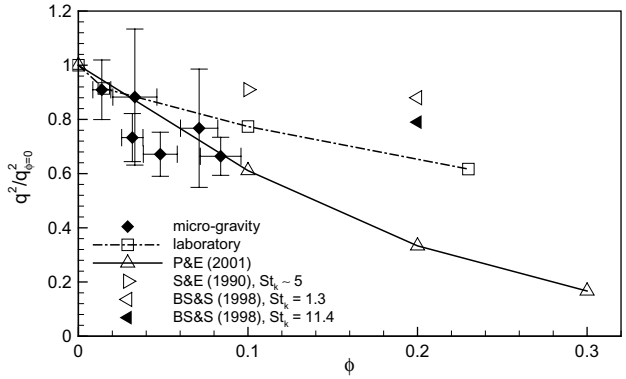

Fig. 3. Attenuation of turbulence kinetic energy with particles. The micro-gravity results are compared with laboratory measurements, turbulent channel flow centerplane data of Paris and Eaton (2001), and stationary homogeneous and isotropic turbulence DNS data (in the absence of gravity) of Squires and Eaton (1990) and Boivin et al. (1998).

general trend of increasing attenuation with increasing mass loading, similar to the grid-generated turbulence experiments of Geiss et al. (2004), where the turbulence is approximately homogeneous and isotropic in planes parallel to the grid. For the present experiments, the highest mass loading was 0.084, but even that light loading resulted in a 34% reduction of the turbulence kinetic energy. Although the uncertainty of the micro-gravity results is relatively large, there appears to be a consistent trend of greater turbulence attenuation for the micro-gravity case relative to the ground-based experiments. This is an indication that the absence of flow disturbances caused by settling particles (e.g. wakes) enhanced the effects of turbulence attenuation, as there was no additional input of energy to the flow due to particle potential energy loss. The attenuation might have been due to small-scale 'extra dissipation' near the particle surfaces and large-scale flow structure distortion caused by the relatively stationary dispersion of particles hindering the evolution of the turbulence.

It is interesting to note that the micro-gravity turbulence attenuation data seemed to follow the trend of the turbulent channel flow centerplane data of Paris and Eaton (2001), where the turbulence was approximately homogeneous and isotropic, and the turbulence kinetic energy was diffused toward the centerplane from near the wall. DNS of stationary homogeneous and isotropic turbulence in the absence of gravity by Squires and Eaton (1990) and Boivin et al. (1998) could not capture the extent of attenuation observed in our experiments. This was probably due to the limitations of force-coupling schemes in their numerical simulations.

3.2. Detailed results from the first data set

Representative results from one parabola will be presented here, as the results from the different parabolas looked similar. The data set from the first parabola was chosen, because the number of image pairs was larger than that of most of the other parabolas, and most of the particles were dispersed to give a relatively higher ϕ than that of the other parabolas. This parabola included 18 valid image pairs acquired at a mass loading of 0.048.

Fig. 4 indicates that a coherent secondary flow with mean velocities of $\bar{u}_1 = -0.044$ m/s and $\bar{u}_2 = -0.38$ m/s could be observed by averaging over 18 image pairs. The horizontal mean velocity was small as expected. The relatively stronger $\bar{u}_2$ and resultant spatial gradients were probably not representative of the actual secondary flow in the chamber, but most likely due to a few fluid downward motion events captured in the relatively small number of images. As can be seen from the large uncertainty in the turbulence kinetic energy measurements, relatively large measurement uncertainties arise from the small number of images. It should be noted that Hwang and Eaton (2004a) reported mean velocities that were less than about 10% of the rms velocities in the same facility for unladen turbulence when 1000 image pairs were taken. The secondary flow is probably due to slight unbalancing of the speakers or the chamber not being perfectly symmetric.

The mean velocity was subtracted from the velocity vectors to obtain the fluctuating velocities, and then normalized by the rms velocity to obtain the fluctuating fluid velocity probability density functions (PDF)

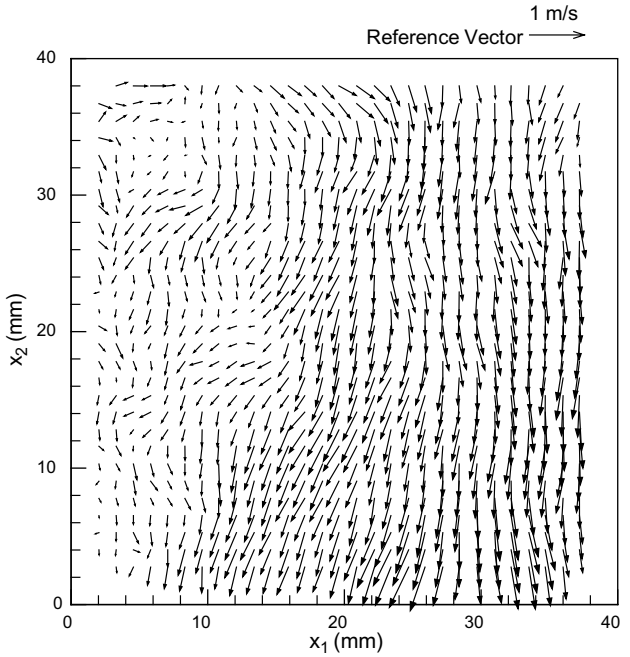

Fig. 4. Mean fluid velocity field of the data set for the first parabola in micro-gravity.

in Fig. 5. The PDFs indicated that both the horizontal and vertical velocity components had nearly Gaussian distributions. The PDFs were a bit noisy due to the small number of flow realizations. The horizontal and vertical rms fluid velocities were similar at 0.757 and 0.742 m/s, respectively, indicating that the flow remained isotropic even as the turbulence was attenuated. The PDF of the shear stress correlation coefficient, $\overline{u_1' u_2'}/(u_{1,\mathrm{rms}} u_{2,\mathrm{rms}})$, in Fig. 6 had a peak centered at zero and a small average value of 0.0367. This was another indication that the turbulence was isotropic.

Spatial energy spectra were obtained from the two-dimensional PIV measurements using the method outlined by Liu et al. (1994, 1999). The radial energy-spectrum function is defined as (Hwang and Eaton, 2004a)

$$E(k) = \frac{k}{2} \int_0^{2\pi} (\Delta k)^2 \langle \hat{u}_i'(k) \hat{u}_i'^{*}(k) \rangle \mathrm{d}\theta \tag{3.5}$$

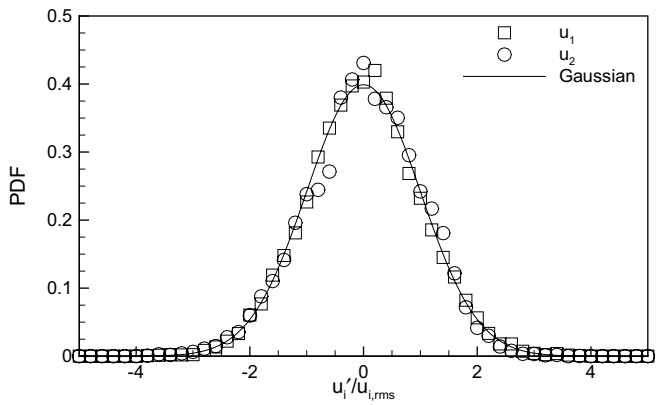

Fig. 5. Fluctuating fluid velocity PDFs of the first data set.

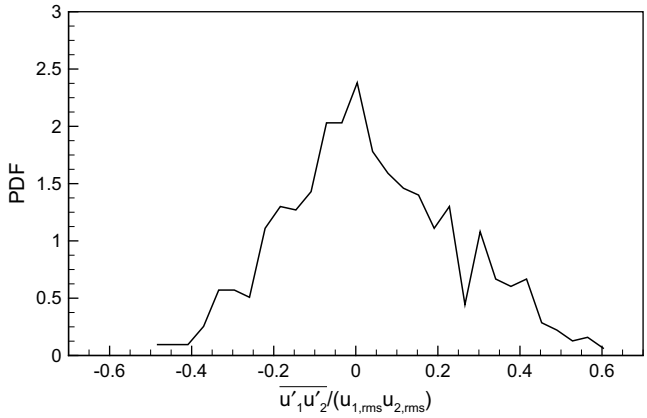

Fig. 6. Shear stress correlation coefficient PDF of the first data set.

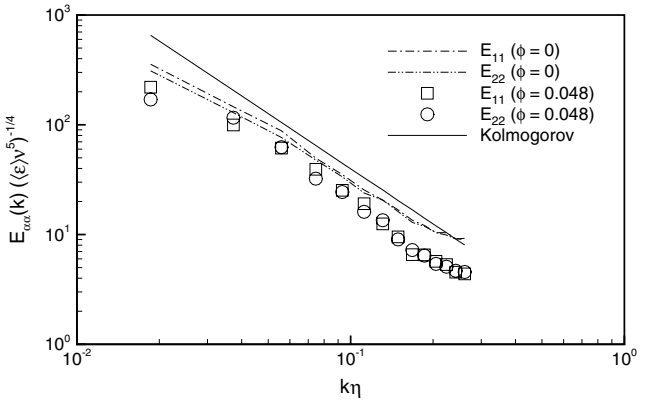

Fig. 7. Radial energy spectra for the first data set, compared with the base unladen data set and the Kolmogorov −5/3 spectrum.

where k is the wavenumber, the first factor in the integrand is the square of the annulus width in wavenumber space, and the second factor in the integrand is the average squared modulus of Fourier transformed fluctuating velocities. Radial energy spectra for the horizontal and vertical velocity components are plotted against the wavenumber normalized by the unladen Kolmogorov length scale η in Fig. 7, along with the Kolmogorov −5/3 spectrum. The agreement with the −5/3 slope suggested that part of the inertial range was being observed. The spectra for both velocity components were attenuated throughout the measurable wavenumber range, compared to the base unladen case. The level of attenuation was slightly greater for the higher wavenumbers, probably due to individual particles extracting energy at small length scales. This was contrary to the grid-generated turbulence experiments of Poelma et al. (2006), where the relative energy at high wavenumbers was augmented. Both velocity components had similar spectral values, indicating that the flow was relatively isotropic.

4. Discussion and conclusions

We have examined turbulence attenuation by particles for the simplest possible case, namely isotropic turbulence with no mean particle or fluid velocity. The particle parameters were selected to be in the range that has been observed to cause strong attenuation. The experiments mimic a number of previous numerical simulations that were done using direct numerical simulation of the Navier–Stokes equations augmented with a point-force model to represent the particle-turbulence interaction. While the present experimental results are subject to relatively large experimental uncertainty, the degree of turbulence attenuation is significantly greater

than that predicted by the simulations. Spectral measurements show that the attenuation occurs uniformly across the measured range of turbulence scales.

Hwang and Eaton (2006) conducted similar experiments under terrestrial gravity in the same facility. Particles were dropped from a screw feeder into a long particle chute and through the turbulence chamber. Since long running times were possible, very well resolved statistics are available and a more detailed examination of the turbulence interacting with particles was possible. An analysis of the turbulence kinetic energy in the measurement volume showed that energy inputs from the forcing system and from particles losing potential energy were balanced by ordinary viscous dissipation and extra dissipation due to particles. This latter term is essentially a short-circuiting of the turbulence cascade. Particles absorb energy from the turbulence at a wide range of scales and then deliver it back to the fluid as very small-scale flow distortion. In the micro-gravity experiments, the only source of energy is the forcing system so the overall energy input into the turbulence kinetic energy is reduced. On the other hand, we do not expect the extra dissipation term to be strongly modified by particle mean motion. Therefore, it is not surprising that the turbulence attenuation is substantially greater in the micro-gravity case.

A perhaps surprising feature of the present results is the close agreement to the earlier measurements of Paris and Eaton (2001) in the centerplane of fully developed vertical channel flow. That flow is similar to the present measurements in that the turbulence in the centerplane region is nearly isotropic, and the only source of turbulence energy is by turbulent diffusion from surrounding regions. One might expect the results to agree more closely with our aforementioned experiments conducted under terrestrial gravity. However, the global inhomogeneity of the channel flow probably plays a role. Due to inelastic collisions with the rough channel walls, the particles fell at a velocity significantly below their terminal velocity at a speed near the fluid velocity (Benson and Eaton, 2003). If the particles had fallen at their terminal velocity with respect to the flow 'through' the turbulence, the attenuation levels might have been similar to the terrestrial experiments of Hwang and Eaton (2006). The present results suggest that this global inhomogeneity of the channel flow plays a role in the large attenuation observed by Paris and Eaton.

Acknowledgements

This research was supported by NASA Grants NCC3-640 and NAG3-2738 supervised by Dr. Nasser Rashidnia. The authors gratefully acknowledge the assistance of Mr. Patrick Cabral and Dr. Chris Elkins of Stanford, and Mr. John Yaniec from NASA. The Phast Corporation generously donated the PLB-Amp8, and Dr. Donghee Han provided the PIV code.

References

Benson, M.J., Eaton, J.K., 2003. The effects of wall roughness on the particle velocity field in a fully developed channel flow. Report TSD-150, Department of Mechanical Engineering, Stanford University, California.

Boivin, M., Simonin, O., Squires, K.D., 1998. Direct numerical simulation of turbulence modulation by particles in isotropic turbulence. J. Fluid. Mech. 375, 235–263.

Boivin, M., Simonin, O., Squires, K.D., 2000. On the prediction of gas–solid flows with two-way coupling using large eddy simulation. Phys. Fluids 12, 2080–2090.

Chen, J.-H., Wu, J.-S., Faeth, G.M., 2000. Turbulence generation in homogeneous particle-laden flows. AIAA J. 38, 636–642.

Fallon, T., Rogers, C.B., 2002. Turbulence-induced preferential concentration of solid particles in microgravity conditions. Exp. Fluids 33, 233–241.

Geiss, S., Dreizler, A., Stojanovic, Z., Chrigui, M., Sadiki, A., Janicka, J., 2004. Investigation of turbulence modification in a non-reactive two-phase flow. Exp. Fluids 36, 344–354.

Groszmann, D.E., 2001. Stereoscopic measurement of particle dispersion in microgravity turbulent flow. Ph.D. Thesis, Tufts University, Massachusetts.

Han, D., 2001. Study of turbulent nonpremixed jet flames using simultaneous measurements of velocity and CH distribution. Report TSD-134, Department of Mechanical Engineering, Stanford University, California.

Hwang, W., Eaton, J.K., 2004a. Creating homogeneous and isotropic turbulence without a mean flow. Exp. Fluids 36, 444–454.

Hwang, W., Eaton, J.K., 2004b. Modification of homogeneous and isotropic turbulence by solid particles. Report TF-89, Department of Mechanical Engineering, Stanford University, California.

Hwang, W., Eaton, J.K., 2006. Homogeneous and isotropic turbulence modulation by small heavy (St$\sim$50) particles. J. Fluid Mech. 564, 361–393.

Kiger, K.T., Pan, C., 2002. PIV technique for the simultaneous measurement of dilute two-phase flows. J. Fluids Eng. 122, 811–818.
Kulick, J.D., Fessler, J.R., Eaton, J.K., 1994. Particle response and turbulence modification in fully developed channel flow. J. Fluid Mech. 277, 109–134.
Liu, S., Meneveau, C., Katz, J., 1994. On the properties of similarity subgrid-scale models as deduced from measurements in a turbulent jet. J. Fluid Mech. 275, 83–119.
Liu, S., Katz, J., Meneveau, C., 1999. Evolution and modelling of subgrid scales during rapid straining of turbulence. J. Fluid Mech. 387, 281–320.
Mizukami, M., Parthasarathy, R.N., Faeth, G.M., 1992. Particle-generated turbulence in homogeneous dilute dispersed flows. Int. J. Multiphase Flow 18, 397–412.
Nishino, K., Matsushita, H., 2004. Columnar particle accumulation in homogeneous turbulence. In: Proceedings of fifth International Conference on Multiphase Flows.
Paris, A.D., Eaton, J.K., 2001. Turbulence attenuation in a particle-laden channel flow. Report TSD-137, Department of Mechanical Engineering, Stanford University, California.
Parthasarathy, R.N., Faeth, G.M., 1990. Turbulence modulation in homogeneous dilute particle-laden flows. J. Fluid Mech. 220, 485–514.
Poelma, C., Westerweel, J., Ooms, G., 2006. Turbulence statistics from optical whole-field measurements in particle-laden turbulence. Exp. Fluids 40, 347–363.
Pope, S.B., 2000. Turbulent Flows. Cambridge University Press.
Schreck, S., Kleis, S., 1993. Modification of grid-generated turbulence by solid particles. J. Fluid Mech. 249, 665–688.
Sheng, J., Meng, H., Fox, R.O., 2000. A large eddy PIV method for turbulence dissipation rate estimation. Chem. Eng. Sci. 55, 4423–4434.
Squires, K.D., Eaton, J.K., 1990. Particle response and turbulence modification in isotropic turbulence. Phys. Fluids A 2, 1191–1203.